Complex Gaussian Scale Mixtures of Complex Wavelet Coefficients

Yothin Rakvongthai, *Student Member, IEEE*, An P. N. Vo, *Student Member, IEEE*, and Soontorn Oraintara, *Senior Member, IEEE*

***Abstract*—In this paper, we propose the complex Gaussian scale mixture (CGSM) to model the complex wavelet coefficients as an extension of the Gaussian scale mixture (GSM), which is for real-valued random variables to the complex case. Along with some related propositions and miscellaneous results, we present the probability density functions of the magnitude and phase of the complex random variable. Specifically, we present the closed forms of the probability density function (pdf) of the magnitude for the case of complex generalized Gaussian distribution and the phase pdf for the general case. Subsequently, the pdf of the relative phase is derived. The CGSM is then applied to image denoising using the Bayes least-square estimator in several complex transform domains. The experimental results show that using the CGSM of complex wavelet coefficients visually improves the quality of denoised images from the real case.**

***Index Terms*—Complex Gaussian scale mixtures (CGSMs), complex wavelets, magnitude, phase.**

I. Introduction

IT IS admitted that statistical modeling in the wavelet domain is favorable for many image-processing applications, such as denoising, compression, and classification, because of the wavelet's capability of analyzing and representing images. This ability can be further improved by using complex-valued wavelets rather than real-valued wavelets. It is mainly because the complex wavelets are based on complex-valued sinusoids constituting an analytic signal [1]. Therefore, the real and imaginary parts of a complex-valued wavelet form a Hilbert transform pair. In addition, the advantages of complex wavelets over real wavelets are directly related to the complex magnitude and phase. For example, the magnitude of a complex coefficient possesses the shift-invariance property while a real wavelet coefficient is shift varying. Furthermore, it is well known that the magnitude of a complex wavelet coefficient better represents a singularity than either the real/imaginary part of the complex coefficient or the value of a real wavelet coefficient. Besides magnitude information, phase information plays a key role in image processing as well. A famous example that shows the importance of phase is in [2], where the Fourier phase is shown to contain more information about image features than the magnitude. Moreover, there is also a connection between the phase of a complex wavelet coefficient and image features, such as edges. Specifically, the phase of a complex coefficient in each scale near an edge varies linearly with its distance to the edge [3]. In addition, the coefficient phases across scales at an edge are aligned [4], [5]. These intrascale and interscale relationships have been used in some image-processing applications (e.g., in [3]–[7]). All of these point out the significance of the magnitude and phase information of complex coefficients. In the probabilistic framework, an appropriate model for complex random variables is required to fully utilize complex wavelet coefficients as well as their magnitude and phase information.

Indeed, the probability density function (pdf) of a complex random vector (as a general form of a complex random variable) is the joint pdf of two real-valued random vectors representing the real and imaginary parts. In order to express the pdf of a complex random vector as an analytic function of the complex vector itself, we need an additional assumption. For a class of distributions whose pdfs depend only on the covariance matrix, such as the Gaussian distribution, the assumption is that the covariance matrices of the real and imaginary parts are equal, and that the sum of the two cross-covariance matrices is zero. With such an assumption, the pdf of a complex random vector whose real and imaginary parts are jointly Gaussian can be expressed as a function of a complex vector, and has been studied in [8]–[10] as the complex Gaussian pdf.

There are a number of research studies on the statistical modeling based on complex wavelets. For instance, in [11], the complex hidden Markov tree (CHMT) model is proposed for complex coefficients obtained from the dual-tree complex wavelet transform (DT-$\mathbb{C}$WT) [12]. The bivariate model with the bivariate shrinkage in [13] and the bivariate α-stable distribution in [14] are used for image denoising. In [15], the Cartesian and polar forms of marginal densities of DT-$\mathbb{C}$WT coefficients due to the Gaussian signals are studied. In [16], the complex generalized Gaussian distribution (CGGD) is used for image modeling in the complex wavelet domain.

The Gaussian scale mixture (GSM) [17] model characterizes the set of real-valued random vectors that can be expressed as the product of a zero-mean Gaussian random vector and an independent positive random variable (i.e., a GSM random vector is a mixture of a possibly infinite number of zero-mean Gaussian random vectors). The GSM distribution encompasses many known distributions as special cases, such as the Student's t-distribution, the α-stable distribution, the generalized

Manuscript received July 21, 2009; accepted February 11, 2010. Date of publication March 25, 2010; date of current version June 16, 2010 The associate editor coordinating the review of this manuscript and approving it for publication was Dr. Ivan W. Selesnick.

Y. Rakvongthai and S. Oraintara are with the Department of Electrical Engineering, University of Texas at Arlington, Arlington, TX 76019 USA (e-mail: yothin.rakvongthai@mavs.uta.edu; oraintar@uta.edu).

A. P. N. Vo is with the Feinstein Institute for Medical Research, North Shore LIJ Health System, Manhasset, NY 11030 USA (e-mail: anphuocnhu.vo@mavs.uta.edu).

Color versions of one or more of the figures in this paper are available online at http://ieeexplore.ieee.org.

Digital Object Identifier 10.1109/TSP.2010.2046698

Gaussian distribution (GGD), and the symmetrized Gamma distribution [17], [18]. In [18] and [19], the GSM model is used for wavelet-based statistical modeling of natural images. It can accurately capture both marginal statistics which have peaky and heavy tailed characteristics and joint statistics of wavelet coefficients. Besides the GSM, other wavelet-based image models are also used to capture the characteristics, including the GGD [20], the hidden Markov tree (HMT) model [21], the bivariate model [13], the Bessel K form density [22], the multivariate GGD [23], the multivariate Laplacian distribution [24], and multivariate prior models [25] as examples. In addition, the GSM modeling in the wavelet domain has been used for image denoising in [26], which provides a high-quality image denoising algorithm. Thanks to the usefulness of the GSM model and the complex wavelet transforms, the modification of the GSM for complex coefficients should be beneficial. Nevertheless, to the best of the authors' knowledge, the extension of the GSM to the complex case and its use for statistical modeling in the complex wavelet domain have not been studied yet.

In this paper, we introduce the complex Gaussian scale mixture (CGSM) as an extension of the GSM, which is for real-valued random vectors, to the complex case and use it to model complex wavelet coefficients. To begin with, we discuss the modeling of the real/imaginary part of complex coefficients by the GSM. We then show that the corresponding joint covariance matrix satisfies the circular condition. Assuming that the real part is a GSM, we then prove that the imaginary part is also a GSM with the same multiplier. Accordingly, the CGSM of complex wavelet coefficients is proposed. In addition, some related propositions of the CGSM are presented. Due to the importance of magnitude and phase information of complex wavelets, examples of using the CGSM to derive two pdfs related to the magnitude and phase are also discussed. To show the effectiveness of the CGSM, image denoising is performed using the Bayes least-squares (BLS) estimator with the proposed model. The results show that using the CGSM of complex wavelet coefficients visually improves the quality of denoised images from using the GSM of real wavelet coefficients.

Recently, there are also wavelet-based models extended from the GSM (e.g., the space variant GSM [27], the oriented-adaptive GSM [28], and the GSM for derotated complex coefficients [29]). Nonetheless, those models are outside the scope of this paper and are not discussed herein.

It is worth noting that the framework we discuss herein is not only limited to the DT-$\mathbb{C}$WT [12], which is probably the most widely used complex wavelet transform in image processing, but also includes other complex-valued multiresolution transforms, such as the fast discrete curvelet transform (FDCT) [30], the pyramidal dual-tree directional filter bank (PDTDFB) [31], and the uniform discrete curvelet transform (UDCT) [32]. The derived pdf can be applied and easily extended to other complex transforms because they all behave like complex analytic bandpass filters and, thus, yield complex subband coefficients whose real and imaginary parts correspond to a Hilbert transform pair. As a result, there is a statistical relationship between the real and imaginary parts, which will be studied in this paper. For simplicity, we refer to the complex multiresolution transforms as complex wavelet transforms, and to the corresponding coefficients as complex wavelet coefficients or complex coefficients henceforth.

This paper is organized as follows. Section II discusses the GSM and shows that it can model the real/imaginary part of complex coefficients. In addition, the input-output relationships of the 2-D Hilbert transform in terms of correlation are presented. Using the results from Section II, the CGSM is defined in Section III. In Section IV, some related properties and results are stated. In Section V, image denoising using the Bayes least-square (BLS) estimator of the CGSM is performed. Moreover, the experimental results are shown to illustrate the usefulness of the CGSM. Finally, we conclude this paper in Section VI. The preliminary version of this work is partially described in [33].

II. Statistics of Complex Coefficients

The goal of this section is to study the statistics of the real and imaginary parts of complex coefficients as well as their statistical relationship related to a Hilbert transform pair. In particular, we will show that the GSM can be used to model the real/imaginary part, and that both parts are related in terms of covariance matrices in Subsections II-A and B, respectively.

A. Gaussian Scale Mixtures

To begin with, we briefly discuss the GSM of real random vectors, and empirically show that the real and imaginary parts are consistent with this model.

A random vector $\mathbf{X}$ with dimension N can be characterized by a GSM if it can be expressed as

$$\mathbf{X} = \sqrt{S}\tilde{\mathbf{X}} \tag{1}$$

where $\tilde{\mathbf{X}}$ is a zero-mean Gaussian random vector with covariance matrix $\mathbf{C}_{\tilde{\mathbf{X}}}$, and S is an independent positive scalar random variable called the multiplier or hidden multiplier. For $\mathbf{X}$ to have the unique GSM representation as in (1), the mean of S must be specified. Without loss of generality, we can assume that S has unit mean [26] (i.e., $E[S] = 1$). This implies that the covariance matrix $\mathbf{C}_{\mathbf{X}} = E[S]\mathbf{C}_{\tilde{\mathbf{X}}} = \mathbf{C}_{\tilde{\mathbf{X}}}$. Accordingly, the pdf of $\mathbf{X}$ is given by [26]

$$\begin{aligned} f_{\mathbf{X}}(\mathbf{x}) &= \int_0^\infty f_{\mathbf{X}|S}(\mathbf{x}|s) f_S(s) ds \\ &= \int_0^\infty \frac{\exp\left(-\frac{\mathbf{x}^T(s\mathbf{C}_{\tilde{\mathbf{X}}})^{-1}\mathbf{x}}{2}\right)}{(2\pi)^{\frac{N}{2}}\sqrt{|s\mathbf{C}_{\tilde{\mathbf{X}}}|}} f_S(s) ds \end{aligned} \tag{2}$$

for $\mathbf{x} \in \mathbb{R}^N$, where $\mathbf{x}^T$ is the transpose of $\mathbf{x}$, and $|\mathbf{C}_{\tilde{\mathbf{X}}}|$ is the determinant of $\mathbf{C}_{\tilde{\mathbf{X}}}$. Note that $f_{\mathbf{X}}(\mathbf{x})$ is a Gaussian pdf when $f_S(s)$ is an impulse function. For the choices of the pdf of the multiplier, we refer to [26].

Next, we validate the GSM modeling of the real and imaginary parts of complex coefficients, which is an assumption we will use in Section III. To verify this, we study the marginal statistics of complex coefficients produced by using the UDCT of the Lena image. The log of the normalized marginal histogram of the real/imaginary part of complex coefficients along with its

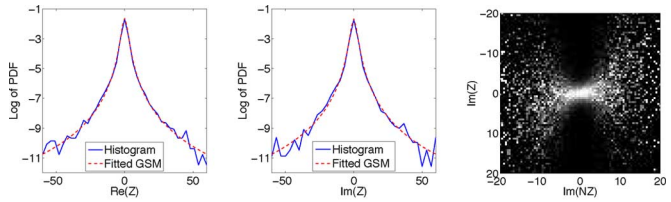

Fig. 1. Marginal and joint statistics of the real/imaginary part of complex coefficients in one finest subband of the Lena image. (a) Log of the normalized marginal histogram and the fitted GSM for the real part. (b) For the imaginary part. (c) The conditional histogram of the imaginary part of two spatially adjacent coefficients Z and its adjacent neighbor NZ. Each column has been independently rescaled to fulfill the full range of intensities. (a) $\Delta H/H = 0.00077$. (b) $\Delta H/H = 0.00107$. (c) $\mathrm{Im}(Z)|\mathrm{Im}(NZ)$.

best fitted Student's t-distribution, which is a class of GSMs, whose hidden multiplier has the inverse Gamma pdf [34] is shown in Fig. 1(a) and (b) for the real and imaginary parts, respectively. Fitting is performed by minimizing the relative entropy ΔH [the Kullback–Leibler divergence (KLD)] between the histogram and the pdf. We can see that the histogram is highly non-Gaussian with high peak at zero, and that the fitting result for each histogram is quite good with the ratio between the KLD and the histogram entropy $\Delta H/H = 0.00077$ and 0.00107 for the real and imaginary parts, respectively. Note also that the marginal distributions of both parts are close to each other. In addition to the marginal statistics, the conditional histogram of two spatially adjacent coefficients is shown in Fig. 1(c). We consider only the imaginary part because the result of the real part is also similar. The shape of this conditional histogram is the so-called bow-tie shape, which implies that two random variables are roughly uncorrelated but highly dependent. These statistical characteristics of the imaginary part of complex coefficients can be modeled by a GSM [18], [19], [26].

B. Hilbert Transform Pairs and Correlation Relationships

Since the real and imaginary parts of complex coefficients are obtained from sampling two processes, which form a Hilbert transform pair, their relationship is crucial to the development of the CGSM, whose pdf is a function of complex variables. In this subsection, we derive the relationship of a 2-D Hilbert transform pair in terms of autocorrelation and cross-correlation, and relate it to the relationship of the real and imaginary parts of complex coefficients. The details are as follows.

Let $X_1(\mathbf{t})$ be a real 2-D random process, where $\mathbf{t} = [t_1, t_2]^T$. The Hilbert transform of $X_1(\mathbf{t})$, which is denoted by $\mathcal{H}\{X_1(\mathbf{t})\}$, is defined as

$$\mathcal{H}\{X_1(\mathbf{t})\} \triangleq (h * X_1)(\mathbf{t})$$

where $h(\mathbf{t})$ is defined by its Fourier transform $H(\boldsymbol{\omega})$ as [35]

$$H(\boldsymbol{\omega}) = -j\mathrm{sgn}(\boldsymbol{\omega}^T\mathbf{e}) = \begin{cases} -j, & \text{if } \boldsymbol{\omega}^T\mathbf{e} > 0; \\ 0, & \text{if } \boldsymbol{\omega}^T\mathbf{e} = 0; \\ j, & \text{if } \boldsymbol{\omega}^T\mathbf{e} < 0 \end{cases} \tag{3}$$

where $\boldsymbol{\omega} = [\omega_1, \omega_2]^T$, and $\mathbf{e} = [e_1, e_2]^T$ is a real unit-norm vector. Let $X_2(\mathbf{t})$ be the Hilbert transform of $X_1(\mathbf{t})$ (i.e., $X_2(\mathbf{t}) = \mathcal{H}\{X_1(\mathbf{t})\}$). Assume that $X_1(\mathbf{t})$ is wide-sense stationary (WSS). Since $\mathcal{H}$ is linear time-invariant (LTI), $X_1(\mathbf{t})$ and $X_2(\mathbf{t})$ are jointly WSS [36], i.e.,

$$E[X_i(\mathbf{t}+\boldsymbol{\tau})X_j(\mathbf{t})] = R_{X_iX_j}(\boldsymbol{\tau})$$

where $\boldsymbol{\tau} = [\tau_1, \tau_2]^T$ for $1 \le i, j \le 2$. Let $R_{X_i}(\boldsymbol{\tau}) \triangleq R_{X_iX_i}(\boldsymbol{\tau})$. The cross power spectrum of two processes $X_i(\mathbf{t})$ and $X_j(\mathbf{t})$ is defined as the Fourier transform $S_{X_iX_j}(\boldsymbol{\omega})$ of $R_{X_iX_j}(\boldsymbol{\tau})$

$$S_{X_iX_j}(\boldsymbol{\omega}) = \int_{\mathbb{R}^2} R_{X_iX_j}(\boldsymbol{\tau}) e^{-j\boldsymbol{\omega}^T\boldsymbol{\tau}} d\boldsymbol{\tau}.$$

When $i = j$, the cross power spectrum becomes the power spectrum (or spectral density) of $X_i(\mathbf{t})$, denoted as $S_{X_i}(\boldsymbol{\omega})$. Note that $S_{X_1X_2}(\boldsymbol{\omega}) = S^*_{X_2X_1}(\boldsymbol{\omega})$ since $X_i(\mathbf{t})$'s are real. Then, we obtain the relationships

$$\begin{aligned} S_{X_2}(\boldsymbol{\omega}) &= S_{X_1}(\boldsymbol{\omega})|H(\boldsymbol{\omega})|^2 \\ S_{X_1X_2}(\boldsymbol{\omega}) &= S_{X_1}(\boldsymbol{\omega})H^*(\boldsymbol{\omega}) \quad \text{and} \\ S_{X_2}(\boldsymbol{\omega}) &= S_{X_1X_2}(\boldsymbol{\omega})H(\boldsymbol{\omega}). \end{aligned} \tag{4}$$

From (3) and (4), it follows that:

$$S_{X_1}(\boldsymbol{\omega}) = S_{X_2}(\boldsymbol{\omega}) \quad \text{and} \quad S_{X_1X_2}(\boldsymbol{\omega}) = -S_{X_2X_1}(\boldsymbol{\omega})$$

and thus

$$R_{X_1}(\boldsymbol{\tau}) = R_{X_2}(\boldsymbol{\tau}) \quad \text{and} \quad R_{X_1X_2}(\boldsymbol{\tau}) = -R_{X_2X_1}(\boldsymbol{\tau}). \tag{5}$$

Consider an N-size neighborhood of each of the real and imaginary parts of complex coefficients. We have the corresponding neighborhood vectors to be

$$\mathbf{X} = [X_1, X_2, \ldots, X_N]^T \quad \text{and} \quad \mathbf{Y} = [Y_1, Y_2, \ldots, Y_N]^T$$

for the real and imaginary parts, respectively. Since the discrete complex wavelet transform can be considered as a bank of bandpass filters, we have $\mathbf{X}$ and $\mathbf{Y}$ as zero-mean. Since $\mathbf{X}$ and $\mathbf{Y}$ are obtained from sampling two processes, which form a Hilbert transform pair, it follows from (5) that:

$$\mathbf{C_X} = \mathbf{C_Y} \quad \text{and} \quad \mathbf{C_{XY}} = -\mathbf{C_{YX}} \tag{6}$$

where $\mathbf{C_X} \triangleq E[\mathbf{X}\mathbf{X}^T]$ and $\mathbf{C_{XY}} \triangleq E[\mathbf{X}\mathbf{Y}^T]$.

Note that this condition on the covariance matrices (6) is the so-called circular [37] or proper [38] condition, and a complex random vector that satisfies these conditions on covariance matrices is called circular [37] or proper [38]. The circular condition allows us to express the jointly Gaussian pdf of the real part $\mathbf{X}$ and the imaginary part $\mathbf{Y}$ as the complex Gaussian pdf of the associated complex number $\mathbf{Z} = \mathbf{X} + j\mathbf{Y}$. This will be discussed briefly in Section III-B.

To verify that the complex wavelet coefficients satisfy the circular condition, we decompose an image into three scales by using the UDCT, DT-$\mathbb{C}$WT, PDTDFB, and FDCT. Then, in each subband, we form the 9×1 complex random vector from the

TABLE I
DEGREES OF IMPROPRIETY FOR VARIOUS COMPLEX TRANSFORMS

Image	Scale	UDCT	DT-$\mathbb{C}$WT	PDTDFB	FDCT
Lena	1	0.0741	0.9375	0.1406	0.1892
	2	0.0435	0.0855	0.1482	0.0795
	3	0.0924	0.2340	0.1495	0.0639
Barbara	1	0.0822	0.8882	0.0905	0.1444
	2	0.0372	0.0854	0.0972	0.1112
	3	0.0614	0.1683	0.0712	0.0814

3×3-block neighborhood. To quantitatively measure the circularity of the complex random vector, we compute the degree of impropriety [39] which measures how much a complex random vector is noncircular. For a zero-mean complex random vector $\mathbf{Z} = \mathbf{X} + j\mathbf{Y}$ with complex covariance matrix $\mathbf{C_Z} \triangleq E[\mathbf{Z}\mathbf{Z}^H]$, where $\mathbf{Z}^H = (\mathbf{Z}^*)^T$ is the conjugate transpose of $\mathbf{Z}$, and pseudocovariance matrix $\mathbf{P_Z} \triangleq E[\mathbf{Z}\mathbf{Z}^T]$, the degree of impropriety is defined by [39]

$$d = 1 - \frac{|\bar{\mathbf{R}}|}{|\mathbf{C_Z}|^2} \tag{7}$$

where $\bar{\mathbf{R}} = \begin{bmatrix} \mathbf{C_Z} & \mathbf{P_Z} \\ \mathbf{P_Z^*} & \mathbf{C_Z^*} \end{bmatrix}$. The value of the degree of impropriety d is between zero and one, where $d = 0$ when the complex random vector is circular and least circular when $d = 1$.

Table I shows the degrees of impropriety for the Lena, and Barbara images. For each image, we compute the degree of impropriety of each subband using (7). Each entry is the average value of the degrees of impropriety of all subbands in one scale. From Table I, for the UDCT, PDTDFB, and FDCT, we can see that the average degrees of impropriety in all three scales of each transform are small (i.e., the UDCT, PDTDFB, and FDCT coefficients can be assumed to satisfy the circular condition). This is also true for the DT-$\mathbb{C}$WT in scales 2 and 3, whereas in the first scale, the degrees of impropriety are quite large ($d > 0.88$ for both images), which implies that the DT-$\mathbb{C}$WT coefficients in the finest scale do not satisfy the circular condition. This is because in the implementation of the DT-$\mathbb{C}$WT, we lose the analyticity of the scale 1 filters to achieve the approximate analyticity at other scales [1].

III. COMPLEX GAUSSIAN SCALE MIXTURES

To exploit the advantages of complex wavelets and the usefulness of the complex magnitude and phase in the statistical framework, an appropriate model that can handle complex random variables is needed. The aim of this section is to introduce the pdf of a vector of complex coefficients whose real and imaginary parts are GSMs because of the effectiveness of the GSM model in statistical wavelet modeling as mentioned earlier.

A. Equivalence of the Hidden Multipliers of the Real and Imaginary Parts

Lemma 3.1: Let $X(\mathbf{n})$ and $Y(\mathbf{n})$ be two random variables of the real and imaginary parts of the complex subband coefficient at position $\mathbf{n}$, respectively. If $X(\mathbf{n})$ is a GSM with constant scalar multiplier in the neighborhood of $\mathbf{n}$, then $Y(\mathbf{n})$ can be modeled by a GSM with the same scalar multiplier. □

Proof: Assume that $X(\mathbf{n})$ is a GSM. From (1), $X(\mathbf{n})$ can be written as

$$X(\mathbf{n}) = \sqrt{S_1(\mathbf{n})}\tilde{X}(\mathbf{n})$$

where $\tilde{X}(\mathbf{n})$ is zero-mean Gaussian, $S_1(\mathbf{n})$ is unit-mean and independent to $\tilde{X}(\mathbf{n})$. Since $Y(\mathbf{n})$ is a Hilbert transform pair of $X(\mathbf{n})$, we have

$$Y(\mathbf{n}) = \sum_{\mathbf{m}\in\mathbb{Z}^2} X(\mathbf{n}-\mathbf{m})h(\mathbf{m})$$

where $h(\mathbf{m})$ is the impulse response of a 2-D Hilbert transform. Hence, $Y(\mathbf{n})$ can be approximated by

$$Y(\mathbf{n}) = \sum_{\mathbf{m}\in\mathbb{Z}^2} X(\mathbf{n}-\mathbf{m})h(\mathbf{m}) \approx \sum_{\mathbf{m}\in\mathcal{A}} X(\mathbf{n}-\mathbf{m})h(\mathbf{m})$$

where $\mathcal{A}$ is the set of points $\mathbf{m}$ so that $\mathbf{n}-\mathbf{m}$ is in the neighborhood of $\mathbf{n}$. Since $\mathbf{m} \in \mathcal{A}, S_1(\mathbf{n}-\mathbf{m}) = S_1(\mathbf{n})$. Hence, we have

$$\begin{aligned} Y(\mathbf{n}) &\approx \sum_{\mathbf{m}\in\mathcal{A}} \sqrt{S_1(\mathbf{n}-\mathbf{m})}\tilde{X}(\mathbf{n}-\mathbf{m})h(\mathbf{m}) \\ &= \sqrt{S_1(\mathbf{n})} \sum_{\mathbf{m}\in\mathcal{A}} \tilde{X}(\mathbf{n}-\mathbf{m})h(\mathbf{m}) = \sqrt{S_1(\mathbf{n})}\tilde{Y}(\mathbf{n}) \end{aligned}$$

where $\tilde{Y}(\mathbf{n}) = \sum_{\mathbf{m}\in\mathcal{A}} \tilde{X}(\mathbf{n}-\mathbf{m})h(\mathbf{m})$ is zero-mean Gaussian and independent to $S_1(\mathbf{n})$. ■

Proposition 3.1: Let $\mathbf{X}$ and $\mathbf{Y}$ be two random vectors of neighborhoods of the real and imaginary parts of complex subband coefficients, respectively. If $\mathbf{X}$ is a GSM, then so is $\mathbf{Y}$ and $\mathbf{X}$ and $\mathbf{Y}$ have the same scalar multiplier. □

Proof: Assume that $\mathbf{X}$ is a GSM. From (1), $\mathbf{X}$ can be written as $\mathbf{X} = \sqrt{S_1}\tilde{\mathbf{X}}$, where $\tilde{\mathbf{X}}$ is zero-mean Gaussian, S_1 are unit-mean and independent to $\tilde{\mathbf{X}}$. It follows directly from Lemma 3.1 that

$$\mathbf{Y} = \sqrt{S_1}\tilde{\mathbf{Y}}$$

where $\tilde{\mathbf{Y}}$ is zero-mean Gaussian independent to S_1 (i.e., $\mathbf{Y}$ is also a GSM with the same hidden multiplier). ■

This result is demonstrated in Fig. 2, where we assume $\mathbf{X} = \sqrt{S_1}\tilde{\mathbf{X}}$ and $\mathbf{Y} = \sqrt{S_2}\tilde{\mathbf{Y}}$, and consider the conditional histogram of S_2 given S_1, $f_{S_2|S_1}(s_2|s_1)$. Due to their hidden structure, the hidden multipliers S_1 and S_2 cannot be observed. However, we can estimate each of them by the maximum-likelihood estimator in each neighborhood [19]

$$\hat{S}_1(\mathbf{x}) = \frac{\mathbf{x}^T\mathbf{C}_{\tilde{\mathbf{X}}}^{-1}\mathbf{x}}{N} \quad \text{and} \quad \hat{S}_2(\mathbf{y}) = \frac{\mathbf{y}^T\mathbf{C}_{\tilde{\mathbf{Y}}}^{-1}\mathbf{y}}{N}$$

where $\mathbf{x}$ and $\mathbf{y}$ are the real and imaginary parts of coefficients in that neighborhood of size N. In Fig. 2, the conditional histograms corresponding to the real and imaginary parts of complex coefficients from one finest subband of the Lena [Fig. 2(a)], and Barbara [Fig. 2(b)] images are shown, where the images are decomposed by using the UDCT. It can be seen that the conditional histograms are densely concentrated around the diagonal line $\hat{S}_1 = \hat{S}_2$ especially when $\hat{S}_1$ is small.

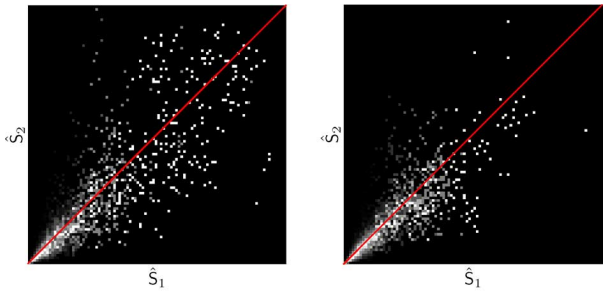

Fig. 2. Conditional histograms of the estimates $\hat{S}_1$ and $\hat{S}_2$ of the hidden multipliers of the real and imaginary parts of complex coefficients from one of the finest subbands of the (a) Lena and (b) Barbara images. Each column has been independently rescaled to fulfill the full range of intensities. The diagonal line in each histogram represents $\hat{S}_1 = \hat{S}_2$. (a) Lena. (b) Barbara.

B. Complex Gaussian Distribution

Before we introduce the CGSM, we discuss the complex Gaussian distribution, which is an important class of the CGSM. Particularly, in this subsection, we present how the pdf of jointly Gaussian random vectors with the circular condition can be written as the pdf of a complex Gaussian vector. For simplicity, we assume the zero-mean case.

To start with, let $\mathbf{X}$ and $\mathbf{Y}$ be two $N \times 1$ zero-mean Gaussian random vectors. Assume that they are jointly Gaussian with the circular condition. Let $\mathbf{U} = [\mathbf{X}^T, \mathbf{Y}^T]^T$, which is Gaussian with covariance matrix $\mathbf{C_U} = \begin{bmatrix} \mathbf{C_X} & \mathbf{C_{XY}} \\ -\mathbf{C_{XY}} & \mathbf{C_X} \end{bmatrix}$, with the pdf given by

$$f_{\mathbf{U}}(\mathbf{u}) = \frac{1}{(2\pi)^{\frac{2N}{2}}\sqrt{|\mathbf{C_U}|}} \exp\left(-\frac{\mathbf{u}^T\mathbf{C_U^{-1}}\mathbf{u}}{2}\right), \quad \text{for } \mathbf{u} \in \mathbb{R}^{2N}. \tag{8}$$

Moreover, its characteristic function has the form

$$\Phi_{\mathbf{U}}(\boldsymbol{v}) \triangleq E[e^{j(\boldsymbol{\alpha}^T\mathbf{X}+\boldsymbol{\beta}^T\mathbf{Y})}] = \exp\left(-\frac{\boldsymbol{v}^T\mathbf{C_U}\boldsymbol{v}}{2}\right) \tag{9}$$

where $\boldsymbol{\alpha}, \boldsymbol{\beta} \in \mathbb{R}^N$, and $\boldsymbol{v} = [\boldsymbol{\alpha}^T, \boldsymbol{\beta}^T]^T$. Let $\mathbf{Z} = \mathbf{X} + j\mathbf{Y}$ with the complex covariance matrix $\mathbf{C_Z} = E[\mathbf{Z}\mathbf{Z}^H]$. Therefore, $\mathbf{C_Z} = 2(\mathbf{C_X} - j\mathbf{C_{XY}})$, and satisfies the following conditions [36], [40].

1) $\mathbf{u}^T\mathbf{C_U^{-1}}\mathbf{u} = 2\mathbf{z}^H\mathbf{C_Z^{-1}}\mathbf{z}$, where $\mathbf{u} = [\mathbf{x}^T, \mathbf{y}^T]^T$ and $\mathbf{z} = \mathbf{x} + j\mathbf{y}$ for all $\mathbf{x}, \mathbf{y} \in \mathbb{R}^N$.
2) $\boldsymbol{v}^T\mathbf{C_U}\boldsymbol{v} = (1/2)\boldsymbol{\omega}^H\mathbf{C_Z}\boldsymbol{\omega}$, where $\boldsymbol{v} = [\boldsymbol{\alpha}^T, \boldsymbol{\beta}^T]^T$ and $\boldsymbol{\omega} = \boldsymbol{\alpha} + j\boldsymbol{\beta}$ for all $\boldsymbol{\alpha}, \boldsymbol{\beta} \in \mathbb{R}^N$.
3) $2^{2N}|\mathbf{C_U}| = |\mathbf{C_Z}|^2$.

Using statements 1) and 3), the Gaussian pdf of $\mathbf{U} = [\mathbf{X}^T, \mathbf{Y}^T]^T$ in (8) can be expressed as the complex Gaussian pdf of $\mathbf{Z} = \mathbf{X} + j\mathbf{Y}$ having the form

$$f_{\mathbf{Z}}(\mathbf{z}) = \frac{\exp\left(-\mathbf{z}^H\mathbf{C_Z^{-1}}\mathbf{z}\right)}{\pi^N|\mathbf{C_Z}|}, \quad \text{for } \mathbf{z} \in \mathbb{C}^N. \tag{10}$$

Using statement 2), the characteristic function of $\mathbf{U}$ in (9) can be written as the characteristic function of $\mathbf{Z}$ which is obtained by

$$\Phi_{\mathbf{Z}}(\boldsymbol{\omega}) \triangleq E[e^{j(\boldsymbol{\alpha}^T\mathbf{X}+\boldsymbol{\beta}^T\mathbf{Y})}] = \exp\left(-\frac{\boldsymbol{\omega}^H\mathbf{C_Z}\boldsymbol{\omega}}{4}\right) \tag{11}$$

where $\boldsymbol{\alpha}, \boldsymbol{\beta} \in \mathbb{R}^N$, and $\boldsymbol{\omega} = \boldsymbol{\alpha} + j\boldsymbol{\beta} \in \mathbb{C}^N$. We refer to [36] and [40] for the proofs and more comprehensive details.

C. Complex Gaussian Scale Mixtures

Proposition 3.1 and the circular condition (6) allow us to express the joint pdf of two real-valued random vectors representing the real and imaginary parts as the pdf of the complex-valued random vector. The details are as follows.

To begin with, let $\mathbf{Z} = \mathbf{X} + j\mathbf{Y} = \sqrt{S}\tilde{\mathbf{Z}}$, where $\tilde{\mathbf{Z}} = \tilde{\mathbf{X}} + j\tilde{\mathbf{Y}}$ is a zero-mean complex Gaussian random vector and the unit-mean S is independent to $\tilde{\mathbf{Z}}$. Therefore, the complex covariance is obtained by $\mathbf{C_Z} = E[\mathbf{Z}\mathbf{Z}^H] = E[S]\mathbf{C}_{\tilde{\mathbf{Z}}} = \mathbf{C}_{\tilde{\mathbf{Z}}}$. It follows from the results in Subsection III-B that $\mathbf{C}_{\tilde{\mathbf{Z}}} = E[\tilde{\mathbf{Z}}\tilde{\mathbf{Z}}^H] = 2(\mathbf{C}_{\tilde{\mathbf{X}}} - j\mathbf{C}_{\tilde{\mathbf{X}}\tilde{\mathbf{Y}}})$. From (10)

$$f_{\tilde{\mathbf{Z}}}(\tilde{\mathbf{z}}) = \frac{\exp\left(-\tilde{\mathbf{z}}^H\mathbf{C}_{\tilde{\mathbf{Z}}}^{-1}\tilde{\mathbf{z}}\right)}{\pi^N|\mathbf{C}_{\tilde{\mathbf{Z}}}|}$$

where N is the neighborhood size. Conditioned on S, $\mathbf{Z}|\{S = s\} = \sqrt{s}\tilde{\mathbf{Z}}$ is complex Gaussian with the complex covariance matrix $\mathbf{C}_{\mathbf{Z}|S} = s\mathbf{C}_{\tilde{\mathbf{Z}}}$. Hence, the pdf of $\mathbf{Z}$ is given by

$$\begin{aligned} f_{\mathbf{Z}}(\mathbf{z}) &= \int_0^\infty f_{\mathbf{Z}|S}(\mathbf{z}|s)f_S(s)ds \\ &= \int_0^\infty \frac{\exp(-\mathbf{z}^H(s\mathbf{C}_{\tilde{\mathbf{Z}}})^{-1}\mathbf{z})}{\pi^N|s\mathbf{C}_{\tilde{\mathbf{Z}}}|} f_S(s)ds \end{aligned} \tag{12}$$

for $\mathbf{z} \in \mathbb{C}^N$. Note that $f_{\mathbf{Z}}(\mathbf{z})$ is a complex Gaussian pdf when $f_S(s)$ is an impulse function. We therefore call $\mathbf{Z}$ a CGSM because of its behavior as a complex Gaussian when conditioned on S.

IV. Some Miscellaneous Results

This section discusses miscellaneous results which stem from the CGSM. Particularly, we address properties of the CGSM, and then discuss some distributions derived using the CGSM.

A. Related Properties

This subsection presents some properties related to the CGSM proposed in Section III. We now start with the characteristic function of the CGSM.

Proposition 4.1: If $\mathbf{Z} = \mathbf{X} + j\mathbf{Y}$ is an N-dimensional CGSM, then the characteristic function of $\mathbf{Z}$ is given by

$$\begin{aligned} \Phi_{\mathbf{Z}}(\boldsymbol{\omega}) &= E[e^{j(\boldsymbol{\alpha}^T\mathbf{X}+\boldsymbol{\beta}^T\mathbf{Y})}] \\ &= \int_0^\infty \exp\left(-\frac{\boldsymbol{\omega}^H(s\mathbf{C_Z})\boldsymbol{\omega}}{4}\right) f_S(s)ds \end{aligned}$$

where $\boldsymbol{\alpha}, \boldsymbol{\beta} \in \mathbb{R}^N, \boldsymbol{\omega} = \boldsymbol{\alpha} + j\boldsymbol{\beta}$, and $\mathbf{C_Z} = E[\mathbf{Z}\mathbf{Z}^H]$. □

Proof: Given $S = s, \mathbf{Z}|S$ is complex Gaussian with complex covariance matrix $\mathbf{C}_{\mathbf{Z}|S} = s\mathbf{C}_{\tilde{\mathbf{Z}}} = s\mathbf{C_Z}$. The proof fol-

lows from the fact that the conditional characteristic function of $\mathbf{Z}$ is given by

$$\Phi_{\mathbf{Z}|S}(\boldsymbol{\omega}) = \exp\left(-\frac{\boldsymbol{\omega}^H(s\mathbf{C}_\mathbf{Z})\boldsymbol{\omega}}{4}\right)$$

which follows from (11). ■

Proposition 4.2: If $\mathbf{Z}$ is an N-dimensional CGSM, then $\mathbf{Z}^*$ is also an N-dimensional CGSM and $\mathbf{AZ}$ is an M-dimensional CGSM, where $\mathbf{A}$ is an $M \times N$ complex constant matrix. □

Proof: The proof is trivial. ■

Before presenting a property of the CGSM, we discuss an analogous property of the GSM that is also mentioned in [41].

Proposition 4.3: If X_1 and X_2 are independent univariate GSMs, then $X_3 = X_1 + X_2, X_4 = X_1X_2$ and $X_5 = X_1/X_2$ are also GSMs. □

Proof: Let $X_i = \sqrt{S_i}\tilde{X}_i$ for $i = 1, 2$, where the unit-mean positive random variable S_i and the zero-mean Gaussian random variable $\tilde{X}_i$ are independent. Assume further that X_1 and X_2 are independent.

Given $S_1 = s_1$ and $S_2 = s_2, X_3|\{S_1 = s_1, S_2 = s_2\}$ is zero-mean Gaussian with variance $s_1\mathrm{Var}[\tilde{X}_1] + s_2\mathrm{Var}[\tilde{X}_2]$. Therefore, we can write $X_3 = \sqrt{S_3}\tilde{X}_3$, where $S_3 = (S_1\mathrm{Var}[\tilde{X}_1] + S_2\mathrm{Var}[\tilde{X}_2])/(\mathrm{Var}[\tilde{X}_1] + \mathrm{Var}[\tilde{X}_2])$ is unit mean and $\tilde{X}_3 \sim \mathcal{N}(0, \mathrm{Var}[\tilde{X}_1] + \mathrm{Var}[\tilde{X}_2])$ independent to S_3.

To show that X_4 is a GSM, consider $X_4 = X_1X_2 = \sqrt{S_1S_2}\tilde{X}_1\tilde{X}_2$. Hence, we can write $X_4 = \sqrt{S_4}\tilde{X}_4$, where $S_4 = (S_1S_2/\mathrm{Var}[\tilde{X}_2])\tilde{X}_2^2$ is unit mean and $\tilde{X}_4 = \sqrt{\mathrm{Var}[\tilde{X}_2]}\mathrm{sgn}(\tilde{X}_2)\tilde{X}_1$ is zero-mean Gaussian independent to S_4.

Finally, we write $X_5 = X_1/X_2 = \sqrt{S_1}\tilde{X}_1/(\sqrt{S_2}\tilde{X}_2)$. Similarly, it can be seen that $X_5 = \sqrt{S_5}\tilde{X}_5$, where $S_5 = S_1/(S_2E[1/S_2]E[1/\tilde{X}_2^2]\tilde{X}_2^2)$ is unit mean, and $\tilde{X}_5 = \sqrt{E[1/S_2]E[1/\tilde{X}_2^2]}\mathrm{sgn}(1/\tilde{X}_2)\tilde{X}_1$ is zero-mean Gaussian independent to S_5. Hence, X_3, X_4, and X_5 are also GSMs. ■

Similar to the GSM, a similar property for the CGSM is found in the following proposition.

Proposition 4.4: If Z_1 and Z_2 are independent univariate CGSMs, then $Z_3 = Z_1 + Z_2, Z_4 = Z_1Z_2$, and $Z_5 = Z_1/Z_2$ are also CGSMs. □

Proof: Let $Z_i = \sqrt{S_i}\tilde{Z}_i$ for $i = 1, 2$ where the unit-mean positive random variable S_i and the zero-mean complex Gaussian random variable $\tilde{Z}_i$ are independent. For $i = 1, 2$, we can write $Z_i = X_i + jY_i$, where X_i and Y_i are GSMs with $X_i = \sqrt{S_i}\tilde{X}_i$ and $Y_i = \sqrt{S_i}\tilde{Y}_i$. Assume further that Z_1 and Z_2 are independent. Therefore, $[X_1, Y_1]$ and $[X_2, Y_2]$ are independent. We then write

$$\begin{aligned}
Z_3 &= Z_1 + Z_2 = (X_1 + X_2) + j(Y_1 + Y_2) \\
&\triangleq X_3 + jY_3, \\
Z_4 &= Z_1Z_2 = (X_1X_2 - Y_1Y_2) + j(X_1Y_2 + X_2Y_1) \\
&\triangleq X_4 + jY_4, \\
Z_5 &= Z_1/Z_2 = \frac{X_1X_2 + Y_1Y_2}{X_2^2 + Y_2^2} + j\frac{X_2Y_1 - X_1Y_2}{X_2^2 + Y_2^2} \\
&\triangleq X_5 + jY_5.
\end{aligned}$$

From Proposition 4.3 and the fact that $[X_1, Y_1]$ and $[X_2, Y_2]$ are independent, it is easy to show that X_i and Y_i are orthogonal GSMs with the same variance and the same hidden multiplier, for $i = 3, 4, 5$. As a result, Z_3, Z_4, and Z_5 are also CGSMs. ■

In the next two subsections, we exemplify the usefulness of the proposed CGSM for deriving two pdfs related to the magnitude and phase of complex coefficients.

B. Complex Generalized Gaussian Distribution and Its Magnitude PDF

Based on the CGSM model, there is, in general, no closed form for the magnitude pdf owing to the presence of the hidden multiplier. This leads to difficulties in some applications, such as texture retrieval, where the closed form for the KLD between two distributions is desirable [16]. Therefore, we focus on a special case of the CGSM, the complex generalized Gaussian distribution (CGGD), whose real version, the GGD, is widely used to model real-valued wavelet coefficients [20], [42]. In this subsection, we derive of the magnitude pdf of a complex wavelet coefficient characterized by the CGGD. The CGGD has been utilized to model complex SAR images in [43], and complex wavelet coefficients in [16].

Let a complex coefficient $Z = X + jY$ be characterized by the CGSM when $N = 1$ (i.e., $[X, Y]^T$ is a GSM). If $f_S(s)$ is such that $f_{X,Y}(x, y)$ is the pdf of the bivariate GGD [16], [23], then the distribution of Z is a CGGD with the pdf [43]

$$\begin{aligned}
f_Z(z) &= f_{X,Y}(x, y) \\
&= \int_0^\infty \frac{\exp\left(-\frac{x^2+y^2}{2s\sigma^2}\right)}{2\pi s\sigma^2} f_S(s)ds \\
&= \frac{\gamma\Gamma\left(\frac{2}{\gamma}\right)}{2\pi\Gamma^2\left(\frac{1}{\gamma}\right)\sigma^2} e^{-\left(\frac{\Gamma\left(\frac{2}{\gamma}\right)}{2\Gamma\left(\frac{1}{\gamma}\right)}\frac{x^2+y^2}{\sigma^2}\right)^\gamma} \\
&= \frac{\gamma\Gamma\left(\frac{2}{\gamma}\right)}{2\pi\Gamma^2\left(\frac{1}{\gamma}\right)\sigma^2} e^{-\left(\frac{\Gamma\left(\frac{2}{\gamma}\right)}{2\Gamma\left(\frac{1}{\gamma}\right)}\frac{|z|^2}{\sigma^2}\right)^\gamma}
\end{aligned}$$

where $\gamma > 0$ and $\sigma^2 > 0$ are the parameters, and $\Gamma(z) \triangleq \int_0^\infty e^{-t}t^{z-1}dt, z > 0$ is the Gamma function. Note that since the GGD is also known as the exponential power distribution [44], this distribution of Z can be called the complex exponential power distribution. Let $X = R\cos\theta$ and $Y = R\sin\theta$, where $R \geq 0$ and $-\pi \leq \theta < \pi$. Then, the pdf of R is given by [16]

$$\begin{aligned}
f_R(r) &= \int_{-\pi}^{\pi} f_{R,\Theta}(r, \theta)d\theta \\
&= \int_{-\pi}^{\pi} r f_Z(r\cos\theta + jr\sin\theta)d\theta \\
&= \frac{\beta}{\alpha^2\Gamma\left(\frac{2}{\beta}\right)} re^{-\left(\frac{r}{\alpha}\right)^\beta} \qquad (13)
\end{aligned}$$

where $\alpha = \sigma\sqrt{(2\Gamma(1/\gamma))/(\Gamma(2/\gamma))}$, and $\beta = 2\gamma$ are the two parameters. This magnitude pdf (13) is used to model the complex coefficient magnitude and applied to improve the retrieval rate for the texture retrieval application [16].

C. Derivation of the Relative Phase PDF

Although the complex wavelet phase holds crucial information, the coefficient phase in a subband is uniformly distributed, which leads to difficulty in exploiting phase information in the statistical approach. This suggests utilizing the information of a multivariate phase model, such as a bivariate model, rather than a univariate one.

In this subsection, we will use the CGSM to derive the pdf of the relative phase. The relative phase [45] Φ at a spatial location (k,l) is defined as the phase difference of two neighboring complex wavelet coefficients within a particular subband

$$\Phi = \Theta_1 - \Theta_2$$

where Θ_1 is the phase of $Z(k,l)$, the coefficient at position (k,l), and Θ_2 is the phase of $Z(k,l+1)$ (or $Z(k+1,l)$). The relative phase can be derived by assuming that the two adjacent complex coefficients, say Z_1 and Z_2, are characterized by the CGSM [7]. Using $N=2$ for the CGSM pdf in (12), the pdf of the complex random vector $\mathbf{Z} = [Z_1, Z_2]^T$ is given by

$$f_{\mathbf{Z}}(\mathbf{z}) = \int_0^\infty \frac{\exp(-\mathbf{z}^H(\mathbf{C}_{\mathbf{Z}|S})^{-1}\mathbf{z})}{\pi^2|\mathbf{C}_{\mathbf{Z}|S}|} f_S(s)ds.$$

Consequently, the conditional polar form pdf is described by

$$f_{\mathbf{R},\mathbf{\Theta}|S}(r_1,r_2,\theta_1,\theta_2|s) = r_1 r_2 \frac{\exp(-\mathbf{z}^H(\mathbf{C}_{\mathbf{Z}|S})^{-1}\mathbf{z})}{\pi^2|\mathbf{C}_{\mathbf{Z}|S}|}$$

where $Z_i = R_i e^{j\Theta_i}$, for $i=1,2$, and $\mathbf{C}_{\mathbf{Z}|S} = E[\mathbf{Z}\mathbf{Z}^H|s] = s\mathbf{C}_{\tilde{\mathbf{Z}}} = s\begin{bmatrix} a_{11} & a_{12} \\ a_{12}^* & a_{22} \end{bmatrix}$. Let $\mathbf{B} = \begin{bmatrix} b_{11} & b_{12} \\ b_{12}^* & b_{22} \end{bmatrix}$ be the inverse of $\mathbf{C}_{\mathbf{Z}|S}$. Then, the conditional joint pdf of the phases is given by [10]

$$\begin{aligned} f_{\Theta|S}(\theta_1,\theta_2|s) &= \frac{1}{\pi^2}|\mathbf{B}| \int_0^\infty \int_0^\infty r_1 r_2 e^{-r_1^2 b_{11} - r_2^2 b_{22}} \\ &\quad \times e^{-2r_1 r_2 |b_{12}|\cos(\theta_1-\theta_2-\angle b_{12})} dr_1 dr_2 \\ &= \frac{1-\lambda^2}{4\pi^2(1-\gamma^2)}\left(1 - \frac{\gamma \arccos(\gamma)}{\sqrt{1-\gamma^2}}\right) \end{aligned}$$

where

$$\begin{aligned} \lambda &= \frac{|b_{12}|}{\sqrt{b_{11}b_{22}}} = \frac{|sa_{12}|}{\sqrt{s^2 a_{11}a_{22}}} = \frac{|a_{12}|}{\sqrt{a_{11}a_{22}}} \\ \mu &= \angle(-b_{12}) = \angle sa_{12} = \angle a_{12} \end{aligned}$$

and $\gamma = \lambda\cos(\theta_1 - \theta_2 - \mu + \pi)$. Therefore, the joint pdf is obtained by

$$\begin{aligned} f_{\Theta}(\theta_1,\theta_2) &= \int_0^\infty f_{\Theta|S}(\theta_1,\theta_2|s) f_S(s) ds \\ &= \frac{1-\lambda^2}{4\pi^2(1-\gamma^2)}\left(1 - \frac{\gamma \arccos(\gamma)}{\sqrt{1-\gamma^2}}\right). \end{aligned}$$

Hence, the pdf of the relative phase $\Phi = \Theta_1 - \Theta_2$ is given by

$$f_{\Phi}(\phi) = \frac{1-\lambda^2}{2\pi(1-\gamma^2)}\left(1 - \frac{\gamma \arccos(\gamma)}{\sqrt{1-\gamma^2}}\right) \tag{14}$$

where μ and λ are the two parameters of the pdf, and $\gamma = \lambda\cos(\phi - \mu + \pi)$. It should be noted that this pdf (14) is independent from the prior $f_S(s)$ and is, therefore, in the same form as the relative phase pdf for the complex Gaussian. The relative phase pdf (14) is used to parameterize the relative phase which extracts phase information of complex wavelet coefficients. It is then applied to texture image retrieval and improves the accuracy rate in [7].

V. Application in Image Denoising

To show the effectiveness, we fit the proposed CGSM with the complex subband coefficients of an image and use it in image denoising. The details are as follows.

A. Bayes Least-Squares Estimator for CGSM

One of the best methods for image denoising is the Bayes least-squares (BLS) estimator based on the GSM model presented in [26]. For each neighborhood, the reference coefficient at the center of the neighborhood is estimated from the set of observed coefficients. The subband coefficients are real, and the pdf is a function of the real variable. The BLS method based on the GSM model is used to estimate the real subband coefficients. However, if we use a complex wavelet transform which decomposes an image into subbands of complex coefficients, then we need an algorithm that can handle complex numbers. Therefore, with the analogy of the BLS algorithm for the GSM, we will develop the BLS estimator based on the CGSM for estimating the complex coefficients.

Let $\mathbf{V}$ be the random vector corresponding to a neighborhood of N-observed complex coefficients

$$\mathbf{V} = \mathbf{Z} + \mathbf{W}$$

where $\mathbf{Z}$ is an original complex coefficient vector and $\mathbf{W}$ is a complex noise vector in the transform domain. Suppose that $\mathbf{W}$ is a zero-mean complex Gaussian and $\mathbf{Z}$ is a CGSM random vector as shown in (12). It is well known that the Bayes least-squares estimation is the conditional expectation described as follows:

$$\hat{\mathbf{Z}} = E[\mathbf{Z}|\mathbf{V}] = \int_0^\infty f_{S|\mathbf{V}}(s|\mathbf{v}) E[\mathbf{Z}|\mathbf{V}=\mathbf{v}, S=s] ds \tag{15}$$

where $f_S(s)$ is the pdf of the positive scalar random variable S. In our implementation, the integration in (15) is computed numerically, where K is the number of points for s, by

$$E[\mathbf{Z}|\mathbf{V}] = \sum_{k=1}^{K} f_{S|\mathbf{V}}(s_k|\mathbf{v}) E[\mathbf{Z}|\mathbf{V}=\mathbf{v}, S=s_k].$$

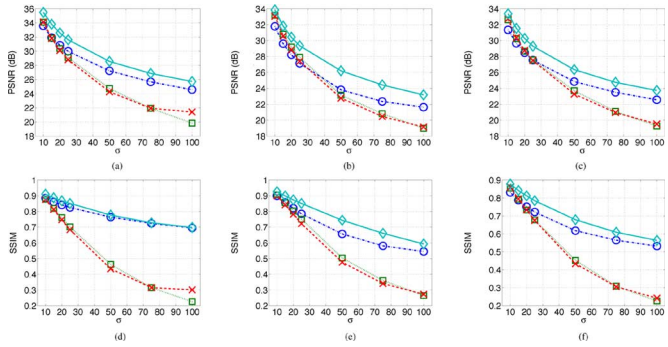

Fig. 3. Denoising performance in terms of PSNR and SSIM for the Lena, Barbara, and Boats images of the HT (∘), GSMsp (□), GSMag (×), and CGSM (♢) methods in the UDCT domain. See text for further information. (a) Lena: PSNR. (b) Barbara: PSNR. (c) Boats: PSNR. (d) Lena: SSIM. (e) Barbara: SSIM. (f) Boats: SSIM.

When conditioned on S and $\mathbf{V}$, the conditional expectation is obtained by

$$E[\mathbf{Z}|\mathbf{V}=\mathbf{v}, S=s] = s\mathbf{C}_{\tilde{\mathbf{Z}}}(s\mathbf{C}_{\tilde{\mathbf{Z}}}+\mathbf{C}_{\mathbf{W}})^{-1}\mathbf{v} \tag{16}$$

where the complex covariance matrices are given by $\mathbf{C}_{\tilde{\mathbf{Z}}} = E[\tilde{\mathbf{Z}}\tilde{\mathbf{Z}}^H]$ and $\mathbf{C}_{\mathbf{W}} = E[\mathbf{W}\mathbf{W}^H]$.

The neighborhood noise covariance matrix $\mathbf{C}_{\mathbf{W}}$ is obtained by decomposing a random noise image which has Gaussian distribution with mean zero, standard deviation σ, and has the same dimension as that of the original image into subbands. Given $\mathbf{C}_{\mathbf{W}}$, the covariance matrix $\mathbf{C}_{\tilde{\mathbf{Z}}}$ can be computed from the observation covariance matrix $\mathbf{C}_{\mathbf{V}}$ (i.e., $\mathbf{C}_{\mathbf{V}} = E[S\tilde{\mathbf{Z}}\tilde{\mathbf{Z}}^H] + E[\mathbf{W}\mathbf{W}^H] = E[S]\mathbf{C}_{\tilde{\mathbf{Z}}} + \mathbf{C}_{\mathbf{W}}$). Since $E[S] = 1$, we have $\mathbf{C}_{\tilde{\mathbf{Z}}} = \mathbf{C}_{\mathbf{V}} - \mathbf{C}_{\mathbf{W}}$. To force the complex covariance matrix to be positive semidefinite, an eigenvalue decomposition of $\mathbf{C}_{\tilde{\mathbf{Z}}}$ is performed and any possible negative eigenvalues are set to zero.

The pdf of the observed neighborhood vector conditioned on S is zero-mean complex Gaussian with covariance $\mathbf{C}_{\mathbf{V}|S} = s\mathbf{C}_{\tilde{\mathbf{Z}}} + \mathbf{C}_{\mathbf{W}}$

$$f_{\mathbf{V}|S}(\mathbf{v}|s) = \frac{\exp(-\mathbf{v}^H(s\mathbf{C}_{\tilde{\mathbf{Z}}}+\mathbf{C}_{\mathbf{W}})^{-1}\mathbf{v})}{\pi^N|s\mathbf{C}_{\tilde{\mathbf{Z}}}+\mathbf{C}_{\mathbf{W}}|}.$$

To estimate $\mathbf{Z}$, $f_{S|\mathbf{V}}(s|\mathbf{v})$ as in (15), it is computed as follows:

$$f_{S|\mathbf{V}}(s|\mathbf{v}) = \frac{f_{\mathbf{V}|S}(\mathbf{v}|s)f_S(s)}{\int_0^\infty f_{\mathbf{V}|S}(\mathbf{v}|\alpha)f_S(\alpha)d\alpha}$$

where we choose the prior $f_S(s)$ to be Jeffrey's noninformative prior [46] for the experiments in this paper. According to Jeffrey's rule, $f_S(s)$ satisfies

$$f_S(s) \propto \sqrt{I(s)}$$

where $I(s)$ is Fisher's information measure which is defined by [46]

$$I(s) = E\left[-\frac{\partial^2 \log f_{\mathbf{Z}|S}(\mathbf{z}|s)}{\partial s^2}\right].$$

For the CGSM model in (12), we have

$$\begin{aligned} -\frac{\partial^2 \log f_{\mathbf{Z}|S}(\mathbf{z}|s)}{\partial s^2} &= \frac{\partial^2}{\partial s^2}\left[N\log(s) + \log|\mathbf{C}_{\tilde{\mathbf{Z}}}| + \frac{\mathbf{z}^H\mathbf{C}_{\tilde{\mathbf{Z}}}^{-1}\mathbf{z}}{s}\right] \\ &= \frac{-N}{s^2} + \frac{2\mathbf{z}^H\mathbf{C}_{\tilde{\mathbf{Z}}}^{-1}\mathbf{z}}{s^3}. \end{aligned}$$

Since $E[\mathbf{z}^H\mathbf{C}_{\tilde{\mathbf{Z}}}^{-1}\mathbf{z}] = s$, by taking the square root of the expectation, we obtain Jeffrey's prior

$$f_S(s) \propto \frac{1}{s}. \tag{17}$$

Note that, in particular, Jeffrey's prior of the CSGM obtained herein is the same as that of the GSM obtained in [26].

B. Experiment Setup

In denoising experiments, we use three standard test images of size 512×512, Lena, Barbara, and Boats. The original image is corrupted by additive white Gaussian noise with a known variance, where the standard deviation of the input noise is varied between $\sigma = 10$ and $\sigma = 100$. First, the noisy image is decomposed into subbands in the transform domain. Each subband except the lowpass subband is denoised. Then, the denoised image is reconstructed from the processed subbands. The denoising performance for each denoised image is evaluated in terms of the peak signal-to-noise ratio (PSNR) value and the structural similarity (SSIM) index [47]. In this paper, the PSNR value (in decibels) is defined as $\mathrm{PSNR} = 20\log_{10}(255/\sigma_\epsilon)$, where σ_ϵ is the error standard deviation.

In our implementation, even though Jeffrey's prior $f_S(s)$ obtained in (17) is an improper pdf, we cope with this fact by setting $f_S(s)$ to be zero in the interval $[0, s_{\min})$ with a small positive value of $s_{\min}$. The points for s are sampled with logarithmically uniform spacing, where we use 13 points of $\log(s)$ over the interval $[\log(s_{\min}), \log(s_{\max})] = [-20.5, 3.5]$ with steps of size two. These parameters for the prior are selected according to [26] for convenient comparison.

C. Experiment 1

First, we compare four methods in the UDCT domain:

1) the proposed CGSM method;
2) the hard thresholding (HT) method;
3) the method where the real and imaginary parts are denoised separately (GSMsp);
4) the method where both parts are formed as the real-valued augmented vectors and are thus denoised simultaneously (GSMag).

In this paper, the UDCT decomposes an image into five scales of oriented subbands: 12 directions in the finest scale and six directions in other scales. For the HT method, the threshold values in each subband are equal to three times the noise standard deviation of that subband. The neighborhood used for this experiment is the 3×3 block without the parent.

The results are displayed in Fig. 3(a)–(c) for the PSNR values, and in Fig. 3(d)–(f) for the SSIM indices. From Fig. 3, we can see that the CGSM method significantly outperforms the HT and GSMsp methods for all three test images in terms of PSNR values and SSIM indices, as expected. It is because the HT method is a much less complicated method where only the coefficient magnitude is considered. Moreover, in the GSMsp method, the real and imaginary parts are denoised separately despite the fact that they are interpreted as the real and imaginary parts of complex coefficients.

Compared with the GSMag method, the CGSM method performs considerably better than the GSMag method. According to the shift-invariance property of complex wavelet transforms, it is suggested that the magnitude (or the complex form) of a complex coefficient should be used (i.e., treating complex coefficients as in the CGSM method is recommended). In fact, there are two equivalent ways to treat circular complex random vectors: treating them as having complex covariance matrices (as in CGSM), or as having real covariance matrices (as in GSMag). It seems that the results of the GSMag method should be as good as those of the CGSM method. Subsequently, it is explained that this is not always true.

In the covariance matrix calculation, once we obtain the signal covariance matrix, we force it to be positive semidefinite. For the case of complex covariance matrices, an eigenvalue decomposition of the complex covariance matrix $\mathbf{C}_{\tilde{\mathbf{Z}}}$ is performed and any possible negative eigenvalues are set to be zero. On the other hand, if we treat the $N \times 1$ complex random vector $\tilde{\mathbf{Z}}$ as the $2N \times 1$ augmented vector of the real and imaginary part vectors $[\tilde{\mathbf{X}}^T, \tilde{\mathbf{Y}}^T]^T$ having the real covariance matrix, we need to set any possible negative eigenvalues of the real covariance matrix $\mathbf{C} = \begin{bmatrix} \mathbf{C}_{\tilde{\mathbf{X}}} & \mathbf{C}_{\tilde{\mathbf{X}}\tilde{\mathbf{Y}}} \\ \mathbf{C}_{\tilde{\mathbf{Y}}\tilde{\mathbf{X}}} & \mathbf{C}_{\tilde{\mathbf{Y}}} \end{bmatrix}$ to be zero. To see this, let $\lambda_1 \geq \lambda_2 \geq \cdots \geq \lambda_{2N}$ be the eigenvalues of $\mathbf{C}$, and $\rho_1 \geq \rho_2 \geq \cdots \geq \rho_N$ be the eigenvalues of $\mathbf{C}_{\tilde{\mathbf{Z}}}$. If the circular condition is satisfied (i.e., if $\mathbf{C}_{\tilde{\mathbf{X}}} = \mathbf{C}_{\tilde{\mathbf{Y}}}$ and $\mathbf{C}_{\tilde{\mathbf{X}}\tilde{\mathbf{Y}}} = -\mathbf{C}_{\tilde{\mathbf{Y}}\tilde{\mathbf{X}}}$), then $\lambda_{2i-1} = \lambda_{2i}$, for $1 \leq i \leq N$, which means that its eigenvalues have even multiplicity [48]. Therefore, the number of possibly negative eigenvalues of $\mathbf{C}$ is even. It also follows from the circularity that we have the relationship $\rho_i = 2\lambda_{2i-1} = 2\lambda_{2i}$, for $1 \leq i \leq N$ [48]. Therefore, the number of negative eigenvalues of $\mathbf{C}$ is an even number, and twice the number of negative eigenvalues of $\mathbf{C}_{\tilde{\mathbf{Z}}}$.

However, in practice, where the circular condition is not ideally satisfied, this condition on the number of negative eigenvalues might not be true. One example of this possibility is given, where the Barbara image is corrupted by additive white Gaussian noise with standard deviation $\sigma = 20$. The neighborhood coefficients are taken from 3×3 blocks in one of the finest subbands of the UDCT decomposition, which results in the 9×9 complex covariance matrix $\mathbf{C}_{\tilde{\mathbf{Z}}}$, and the 18×18 real covariance matrix $\mathbf{C}$. All nine eigenvalues (ρ_i) of $\mathbf{C}_{\tilde{\mathbf{Z}}}$ and 18 eigenvalues (λ_i) of $\mathbf{C}$ are tabulated in Table II. As can be seen, there are five negative eigenvalues of $\mathbf{C}$ (i.e., $\lambda_i, 14 \leq i \leq 18$) that are set to zero while only one eigenvalue ρ_9 of $\mathbf{C}_{\tilde{\mathbf{Z}}}$ is set to zero. As a consequence, the results from using the GSMag method are not as good as (actually much worse than) those results using the CGSM method. Therefore, it is less appropriate to treat the real and imaginary parts of complex coefficients as the augmented vectors having real covariance matrices at least in the image denoising framework as in this paper.

TABLE II
EXAMPLE OF EIGENVALUES OF $\mathbf{C}$ AND $\mathbf{C}_{\tilde{\mathbf{Z}}}$. SEE TEXT FOR DETAILS

Matrix	Eigenvalues					
$\mathbf{C}$	105.18	92.80	54.09	43.41	42.97	26.32
	20.90	19.88	15.75	12.75	6.38	5.89
	3.47	-0.86	-1.09	-3.18	-7.34	-18.23
$\mathbf{C}_{\tilde{\mathbf{Z}}}$	189.92	77.73	53.92	41.18	30.73	12.19
	8.80	6.58	-1.95			

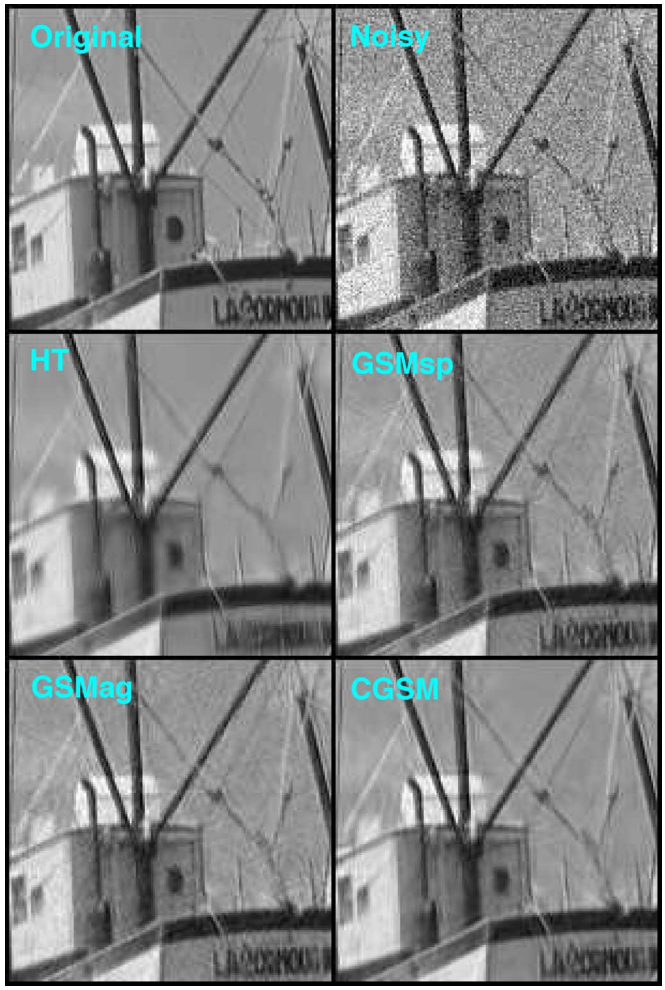

Fig. 4. Denoising performance comparison of the Boats image (cropped to 150×150) with the UDCT. (Top left): original image; (top right): noisy image PSNR 22.11 dB ($\sigma = 20$); (middle left): HT PSNR 28.48 dB; (middle right): GSMsp PSNR 28.68 dB; (bottom left): GSMag PSNR 28.75 dB; (bottom right): CGSM PSNR 30.27 dB.

An example of visual denoising performance using these four methods in the UDCT domain for the Boats image when $\sigma = 20$ is illustrated in Fig. 4. Evidently, the CGSM method yields a visually better denoised image as it retains the image details with less artifacts. Finally, it should be noted that the GSMsp and GSMag methods, which treat complex coefficients inappropriately, yield even worse results for moderate-to-high noise levels than the HT method as can be seen in Fig. 3.

TABLE III
PSNR VALUES (IN DECIBELS) AND SSIM INDICES OF DENOISED IMAGES FROM SEVERAL METHODS

σ	Noisy PSNR	FS GSM	DT-$\mathbb{C}$WT BiShrink	UDCT CGSM	DT-$\mathbb{C}$WT CGSM	PDTDFB CGSM	FDCT CGSM	Noisy SSIM	FS GSM	DT-$\mathbb{C}$WT BiShrink	UDCT CGSM	DT-$\mathbb{C}$WT CGSM	PDTDFB CGSM	FDCT CGSM
Lena														
10	28.13	**35.60**	35.21	35.49	35.50	35.33	35.46	0.614	**0.911**	0.906	0.910	0.910	0.907	0.910
15	24.61	**33.90**	33.50	33.82	33.72	33.57	33.72	0.451	**0.887**	0.881	**0.887**	0.885	0.880	0.886
20	22.11	**32.67**	32.28	32.59	32.40	32.34	32.43	0.344	**0.868**	0.860	**0.868**	0.862	0.858	0.864
25	20.17	**31.69**	31.34	31.62	31.35	31.40	31.42	0.272	0.850	0.841	**0.851**	0.842	0.843	0.844
50	14.15	**28.61**	28.32	28.56	28.06	28.29	28.19	0.113	**0.781**	0.770	0.777	0.761	0.772	0.768
75	10.63	**26.88**	26.52	26.87	26.32	26.48	26.35	0.061	**0.731**	0.716	0.728	0.709	0.716	0.713
100	8.13	25.70	25.29	**25.73**	25.15	25.20	25.07	0.037	0.691	0.674	**0.698**	0.669	0.668	0.669
Barbara														
10	28.13	34.02	33.53	33.85	34.01	33.89	**34.24**	0.716	**0.930**	0.923	0.926	**0.930**	0.925	**0.930**
15	24.61	31.83	31.40	31.83	31.79	31.87	**32.16**	0.579	0.899	0.893	0.899	0.900	0.897	**0.903**
20	22.11	30.27	29.91	30.43	30.25	30.47	**30.70**	0.478	0.869	0.864	0.874	0.870	0.871	**0.878**
25	20.17	29.07	28.76	29.36	29.07	29.41	**29.58**	0.401	0.839	0.837	0.851	0.841	0.846	**0.854**
50	14.15	25.42	25.34	26.21	25.50	26.15	**26.28**	0.196	0.710	0.718	0.744	0.710	0.737	**0.749**
75	10.63	23.61	23.58	24.44	23.60	24.32	**24.46**	0.111	0.622	0.632	0.661	0.617	0.666	**0.668**
100	8.13	22.58	22.50	**23.19**	22.46	23.03	23.16	0.070	0.563	0.572	0.593	0.551	0.597	**0.601**
Boats														
10	28.13	**33.58**	33.22	33.37	33.49	33.28	33.38	0.692	**0.883**	0.876	0.878	0.881	0.878	0.879
15	24.61	**31.69**	31.35	31.54	31.51	31.36	31.48	0.537	**0.845**	0.836	0.842	0.840	0.838	0.840
20	22.11	**30.36**	30.04	30.27	30.13	30.01	30.14	0.426	**0.813**	0.803	0.812	0.805	0.803	0.807
25	20.17	**29.33**	29.03	29.30	29.09	28.99	29.13	0.346	0.784	0.773	**0.785**	0.774	0.772	0.777
50	14.15	26.32	26.02	**26.36**	25.95	26.12	26.08	0.155	0.678	0.665	**0.679**	0.660	0.668	0.668
75	10.63	24.73	24.45	**24.76**	24.33	24.55	24.44	0.086	**0.611**	0.597	0.609	0.586	0.602	0.596
100	8.13	23.72	23.42	**23.74**	23.31	23.50	23.36	0.054	**0.564**	0.550	**0.564**	0.535	0.552	0.545

TABLE IV
REDUNDANCY RATIOS OF THE TRANSFORMS USED HEREIN

Transform	FS	UDCT	DT-$\mathbb{C}$WT	PDTDFB	FDCT
Redund. Ratio	$\approx$18.67	4	4	$\approx$2.67	$\approx$14.53

D. Experiment 2

In this experiment, we first compare image denoising using CGSM with other complex transforms: DT-$\mathbb{C}$WT, PDTDFB, and FDCT. For all complex-valued transforms using the CGSM method, the neighborhood is the 3×3 block without the parent as in the first experiment. For PDTDFB and FDCT, images are decomposed into four scales, while we use five scales for denoising in the DT-$\mathbb{C}$WT domain. These are chosen to produce the best results. The corresponding PSNR values and SSIM indices are tabulated in Table III.

Comparing all complex transforms with the CGSM method, we can see that the UDCT outperforms the other three transforms for the Lena and Boats images in both measures. For the Barbara image, the UDCT performs better than the DT-$\mathbb{C}$WT, and approximately the same as the PDTDFB in both measures. Moreover, we can see that the FDCT outperforms the UDCT in both aspects but it has higher redundancy as shown in Table IV.

We have also compared the CGSM method with the GSM method by using the full steerable pyramid (FS-GSM) with eight directions [26], and the bivariate shrinkage method using the DT-$\mathbb{C}$WT (DT-$\mathbb{C}$WT-BiShrink) [49], which are probably two of the most widely used wavelet-based image denoising methods. For the FS-GSM method, an image is decomposed into five scales. The FS-GSM method outperforms the CGSM method based on complex transforms, including the UDCT-CGSM in PSNR value and SSIM index especially for the Lena and Boats images. On the other hand, for the Barbara image, all complex transforms except the DT-$\mathbb{C}$WT, which provides approximately the same results, yield better denoising results than those yielded by the FS-GSM method in PSNR and SSIM aspects, where the FDCT gives the best results. This is because the Barbara image highly contains oriented line-type structures which can be better represented by the curvelet-like transforms.

We then compare the DT-$\mathbb{C}$WT-BiShrink method with the DT-$\mathbb{C}$WT-CGSM method. Based on the DT-$\mathbb{C}$WT for the Lena and Boats images, the CGSM method performs better than the BiShrink method for low noise levels and vice-versa for high noise levels. However, the BiShrink method is outperformed by the CGSM method for the Barbara image. It should be mentioned that in order to use the CGSM method in the DT-$\mathbb{C}$WT domain, we assume the DT-$\mathbb{C}$WT coefficients in the finest scale satisfy the circular condition although this is not true as we have shown in Section II. Modeling the DT-$\mathbb{C}$WT coefficients in the first scale can improve the results but it is outside the scope of this work as the DT-$\mathbb{C}$WT is used as an example of complex transforms. It is worth noting that the UDCT-CGSM method, however, outperforms the DT-$\mathbb{C}$WT-BiShrink method for all three images.

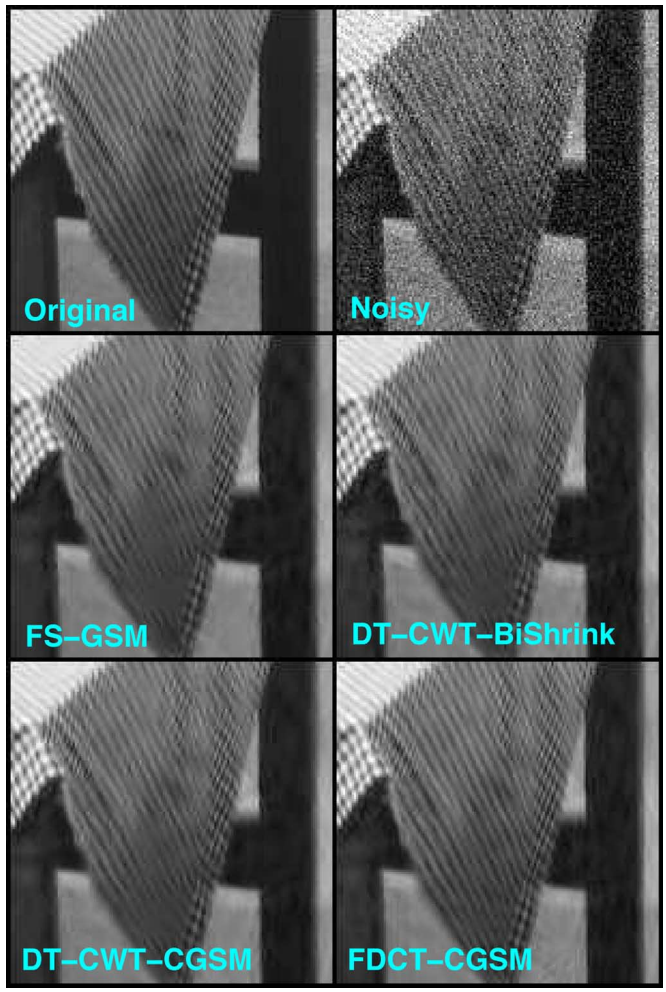

Fig. 5. Denoising performance comparison of the Barbara image (cropped to 150×150). (Top left): original image; (top right): noisy image PSNR 22.11 dB ($\sigma = 20$); (middle left): FS-GSM PSNR 30.27 dB; (middle right): DT-$\mathbb{C}$WT-BiShrink PSNR 29.91 dB; (bottom left): DT-$\mathbb{C}$WT-CGSM PSNR 30.25 dB; and (bottom right): FDCT-CGSM PSNR 30.70 dB.

Fig. 5 shows the visual performance comparison of the Barbara image with several methods. Apparently, the CGSM method especially in the FDCT domain produces the better denoised image in terms of visual quality compared to the FS-GSM and DT-$\mathbb{C}$WT-Bishrink methods. For the Lena and Boats images, the UDCT-CGSM method yields comparable results (≈ -0.05 dB for the PSNR value and ≈ -0.001 for the SSIM index in average) to those of the FS-GSM method but with lower redundancy as shown in Table IV.

VI. Conclusion

We have proposed the CGSM model for complex wavelet coefficients. The real and imaginary parts of the complex coefficients can be modeled by the GSM with the same hidden multiplier. As a consequence, both real and imaginary parts are related in such a way that we can express their joint pdf as a function of complex variables, which we call the pdf of a CGSM. Some related propositions and results of the CGSM are discussed. To illustrate its usefulness, the proposed CGSM is applied to an application in image denoising using the Bayes least-squares (BLS) estimator. The denoising results indicate that the CGSM is a more appropriate model for the complex wavelet coefficients than the joint GSM model of their real and imaginary parts. Moreover, the CGSM allows us to improve the denoising results from those results by using the GSM with the real transforms or obtain comparable results by using a complex transform with less redundancy ratio.

Acknowledgment

The authors would like to thank Dr. T. T. Nguyen for providing his code on the UDCT, and the anonymous reviewers for their constructive comments which greatly improved this paper.

References

[1] I. W. Selesnick, R. G. Baraniuk, and N. G. Kingsbury, "The dual-tree complex wavelet transform," *IEEE Signal Process. Mag.*, vol. 22, no. 6, pp. 123–151, Nov. 2005.

[2] A. V. Oppenheim and J. S. Lim, "The importance of phase in signals," *Proc. IEEE*, vol. PROC-69, no. 5, pp. 529–541, May 1981.

[3] R. Anderson, N. Kingsbury, and J. Fauqueur, "Determining multiscale image feature angles from complex wavelet phases," presented at the ICIAR, Toronto, ON, Canada, Sep. 2005.

[4] P. D. Kovesi, "Image features from phase congruency," *J. Comput. Vis. Res.*, vol. 16, no. 3, Summer 1999.

[5] Z. Wang and E. P. Simoncelli, "Local phase coherence and the perception of blur," *Adv. Neural Inform. Process. Syst.*, vol. 16, 2004.

[6] A. P. N. Vo and S. Oraintara, "A study of relative phase in complex wavelet domain: Property, statistics and applications in texture image retrieval and segmentation," *Signal Process.: Image Commun.*, vol. 25, no. 1, pp. 28–46, Jan. 2010.

[7] A. P. N. Vo, S. Oraintara, and T. T. Nguyen, "Statistical image modeling using distribution of relative phase in the complex wavelet domain," presented at the EUSIPCO, Lausanne, Switzerland, Aug. 2008.

[8] R. A. Wooding, "The multivariate distribution of complex normal variables," *Biometrika*, vol. 4, no. 1–2, pp. 212–215, 1956.

[9] N. R. Goodman, "Statistics analysis based on certain multivariate complex distribution (an introduction)," *Ann. Math. Stat.*, vol. 34, no. 1, pp. 152–177, 1963.

[10] K. S. Miller, "Complex Gaussian processes," *SIAM Rev.*, vol. 11, no. 4, pp. 544–567, Oct. 1969.

[11] H. Choi, J. K. Romberg, R. G. Baraniuk, and N. G. Kingsbury, "Hidden Markov tree modeling of complex wavelet transforms," in *Proc. IEEE ICASSP*, Jun. 2000, vol. 1, pp. 133–136.

[12] N. G. Kingsbury, "Complex wavelets for shift invariant analysis and filtering of signals," *Appl. Computat. Harm. Anal.*, vol. 10, no. 3, pp. 234–253, May 2001.

[13] L. Şendur and I. W. Selesnick, "Bivariate shrinkage functions for wavelet-based denoising exploiting interscale dependency," *IEEE Trans. Signal Process.*, vol. 50, no. 11, pp. 2744–2756, Nov. 2002.

[14] A. Achim and E. E. Kuruoğlu, "Image denoising using bivariate α-stable distributions in the complex wavelet domain," *IEEE Signal Process. Lett.*, vol. 12, no. 1, pp. 17–20, Jan. 2005.

[15] S. M. M. Rahman, M. O. Ahmad, and M. N. S. Swamy, "Statistics of 2-DDT-CWT coefficients for a Gaussian distributed signal," *IEEE Trans. Circuits Syst. I, Reg. Papers*, vol. 55, no. 7, pp. 2013–2025, Aug. 2008.

[16] Y. Rakvongthai and S. Oraintara, "Statistical image modeling with the magnitude probability density function of complex wavelet coefficients," in *Proc. IEEE ISCAS*, Taipei, Taiwan, May 2009, pp. 1879–1882.

[17] D. F. Andrews and C. L. Mallows, "Scale mixtures of normal distributions," *J. Roy. Stat. Soc. B*, vol. 36, no. 1, pp. 99–102, 1974.

[18] M. J. Wainwright, E. P. Simoncelli, and A. S. Willsky, "Random cascades on wavelet trees and their use in analying and modeling natural images," *Appl. Comput. Harm. Anal.*, vol. 11, pp. 89–123, 2001.

[19] M. J. Wainwright and E. P. Simoncelli, "Scale mixtures of Gaussians and the statistics of natural images," *Adv. Neural Inform. Process. Syst.*, vol. 12, pp. 855–861, 2000.

[20] S. G. Mallat, "A theory for multiresolution signal decomposition: The wavelet representation," *IEEE Trans. Pattern Anal. Mach. Intell.*, vol. 11, no. 7, pp. 674–693, Jul. 1989.

[21] M. S. Crouse, R. D. Nowak, and R. G. Baraniuk, "Wavelet-based statistical signal processing using hidden Markov models," *IEEE Trans. Signal Process.*, vol. 46, no. 4, pp. 886–902, Apr. 1998.

[22] J. M. Fadili and L. Boubchir, "Analytical form for a Bayesian wavelet estimator of images using the Bessel K form densities," *IEEE Trans. Image Process.*, vol. 14, no. 2, pp. 231–240, Feb. 2005.

[23] D. Cho and T. D. Bui, "Multivariate statistical modeling for image denoising using wavelet transforms," *Signal Proces.: Image Commun.*, vol. 20, no. 1, pp. 77–89, Jan. 2005.

[24] I. W. Selesnick, "The estimation of Laplace random vectors in addtive white Gaussian noise," *IEEE Trans. Signal Process.*, vol. 56, no. 8, pp. 3482–3496, Aug. 2008.

[25] S. Tan, L. Jiao, and I. A. Kakadiaris, "Wavelet-based Bayesian image estimation: From marginal and bivariate prior models to multivariate prior models," *IEEE Trans. Image Process.*, vol. 17, no. 4, pp. 469–481, Apr. 2008.

[26] J. Portilla, V. Strela, M. J. Wainwright, and E. P. Simoncelli, "Image denoising using scale mixtures of Gaussians in the wavelet domain," *IEEE Trans. Image Process.*, vol. 12, no. 11, pp. 1338–1351, Nov. 2003.

[27] J. A. Guerrero-Colón, L. Mancera, and J. Portilla, "Image restoration using space-variant Gaussian scale mixture in overcomplete pyramids," *IEEE Trans. Image Process.*, vol. 17, no. 1, pp. 27–41, Jan. 2008.

[28] D. K. Hammond and E. P. Simoncelli, "Image modeling and denoising with orientation-adapted Gaussian scale mixtures," *IEEE Trans. Image Process.*, vol. 17, no. 11, pp. 2089–2101, Nov. 2008.

[29] M. Miller and N. Kingsbury, "Image denoising using derotated complex wavelet coefficients," *IEEE Trans. Image Process.*, vol. 19, no. 9, pp. 1500–1511, Sep. 2008.

[30] E. J. Candès, D. L. Donoho, and L. Ying, "Fast discrete curvelet transform," *Multiscale Model. Simul.*, vol. 5, no. 3, pp. 861–899, Sep. 2006.

[31] T. T. Nguyen and S. Oraintara, "The shiftable complex directional pyramid—Part I: Theoretical aspects," *IEEE Trans. Signal Process.*, vol. 56, no. 10, pp. 4651–4660, Oct. 2008.

[32] T. T. Nguyen and H. Chauris, "Uniform discrete curvelet transform for seismic processing," presented at the EAGE Conf. and Tech. Exhibit., Rome, Italy, Jun. 2008.

[33] A. P. N. Vo, T. T. Nguyen, and S. Oraintara, "Image denoising using shiftable directional pyramid and scale mixtures of complex Gaussians," in *Proc. IEEE ISCAS*, New Orleans, LA, May 2007, pp. 4000–4003.

[34] S. Lyu and E. P. Simoncelli, "Nonlinear image representation using divisive normalization," in *Proc. IEEE CVPR*, Anchorage, AK, Jun. 2008, pp. 1–8.

[35] G. H. Granlund and H. Knutsson, *Signal Processing for Computer Vision*. Dordrecht, The Netherlands: Kluwer, 1995.

[36] A. Papoulis and S. U. Pillai, *Probability, Random Variables and Stochastic Processes*. New York: McGraw-Hill, 2002.

[37] B. Picinbono, "Second-order complex random vectors and normal distributions," *IEEE Trans. Signal Process.*, vol. 44, no. 10, pp. 2637–2640, Oct. 1996.

[38] F. D. Neeser and J. L. Massey, "Proper complex random processes with applications to information theory," *IEEE Trans. Inf. Theory*, vol. 39, no. 4, pp. 1293–1302, Jul. 1997.

[39] P. J. Schreier, "Bounds on the degree of impropriety of complex random vectors," *IEEE Signal Process. Lett.*, vol. 15, pp. 190–193, 2008.

[40] S. M. Kay, *Fundamentals of Statistical Signal Processing: Estimation Theory*. Upper Saddle River, NJ: Prentice-Hall, 1993.

[41] H. Hamden, "Characterizing and approximating infinite scale mixtures of normals," *Commun. Stat.-Theory Meth.*, vol. 35, no. 3, pp. 407–413, 2006.

[42] P. Moulin and J. Liu, "Analysis of multiresolution image denoising schemes using generalized Gaussian and complexity priors," *IEEE Trans. Inf. Theory*, vol. 45, no. 3, pp. 909–919, Apr. 1999.
[43] M. S. Davis, P. Bidigare, and D. Chang, "Statistical modeling and ML parameter estimation of complex SAR imagery," in *Proc. Asilomar Conf. Signals, Syst., Comput*, Nov. 2007, pp. 500–502.
[44] S. Kotz, T. J. Kozubowski, and K. Podgórski, *The Laplace Distribution and Generalizations: A Revisit With Applications to Communications, Economics, Engineering, and Finance*. Boston, MA: Birkhäuser, 2001.
[45] A. P. N. Vo, S. Oraintara, and T. T. Nguyen, "Using phase and magnitude information of the complex directional filter bank for texture image retrieval," in *Proc. IEEE ICIP*, San Antonio, TX, Sep. 2007, vol. 4, pp. IV-61–IV-64.
[46] G. E. P. Box and G. C. Tiao, *Bayesian Inference in Statistical Analysis*. Reading, MA: Addison-Wesley, 1973.
[47] Z. Wang, A. C. Bovik, H. R. Sheikh, and E. P. Simoncelli, "Image quality assessment: From error visibility to structural similarity," *IEEE Trans. Image Process.*, vol. 13, no. 4, pp. 600–612, Apr. 2004.
[48] P. J. Schreier and L. L. Scharf, "Second-order analysis of improper complex random vectors and processes," *IEEE Trans. Signal Process.*, vol. 51, no. 3, pp. 714–725, Mar. 2003.
[49] L. Şendur and I. W. Selesnick, "Bivariate shrinkage with local variance estimation," *IEEE Signal Process. Lett.*, vol. 9, no. 12, pp. 438–441, Dec. 2002.

Yothin Rakvongthai (S'07) received the B.Eng. degree (Hons.) in electrical engineering from Chulalongkorn University, Thailand, in 2004, the M.S. degree in electrical engineering from the University of California, Los Angeles, in 2005, and is currently pursuing the Ph.D. degree at the University of Texas at Arlington.

His current research interests include statistical image modeling in the complex wavelet domain and its applications.

Mr. Rakvongthai received a bronze medal from the 41st International Mathematical Olympiad in 2000 and a Lucent Global Science Scholarship from Lucent Technologies, in 2001.

An P. N. Vo (S'08) received the B.S. and M.S. degrees in electrical engineering from HCMC University of Technology in 1997 and 2000, respectively, and the Ph.D. degree in electrical engineering from the University of Texas at Arlington in 2008.

From 2000 to 2004, she was a Lecturer in the Department of Electrical Engineering at the HCMC University of Technology. She joined the Feinstein Institute for Medical Research, North Shore LIJ Health System, NY, as a Postdoctoral Research Fellow in 2009. Her research interests focus on complex wavelet transforms; statistical image modeling; pattern recognition; registration; statistical parametric mapping; quantitative brain imaging; advanced functional brain scanning techniques, such as diffusion tensor imaging (DTI); positron emission tomography (PET); high-field magnetic resonance imaging (MRI) and functional MRI; as well as applications in bioinformatics and biomedical images.

Soontorn Oraintara (S'97–M'00–SM'04) received the B.E. degree (Hons.) in electrical engineering from the King Mongkut's Institute of Technology Ladkrabang, Bangkok, Thailand, in 1995, the M.S. degree in electrical engineering from the University of Wisconsin, Madison, in 1996, and the Ph.D. degree from Boston University, Boston, MA, in 2000.

In 2000, he joined the Department of Electrical Engineering, University of Texas at Arlington (UTA), where he is currently an Associate Professor. From 1998 to 2000, he was an Intern and a Consultant at the Advanced Research and Development Group, Ericsson Inc., Research Triangle Park, NC. His current research interests include digital signal processing: wavelets and multirate systems and their applications in data compression; signal detection and estimation; and statistical modeling. He is an Associate Editor for the IEEE TRANSACTIONS ON SIGNAL PROCESSING.

Dr. Oraintara was the recipient of the Technology Award from Boston University for his invention on integer discrete cosine transform in 1999 and the College of Engineering Outstanding Young Faculty Member Award from UTA in 2003. He represented Thailand in the International Mathematical Olympiad competitions, and, respectively, received the Honorable Mention Award in Beijing, China, in 1990, and the bronze medal in Sigtuna, Sweden, in 1991.